Cement and Concrete Research 41 (2011) 1078–1084

Contents lists available at ScienceDirect

Cement and Concrete Research

journal homepage: http://ees.elsevier.com/CEMCON/default.asp

Study of the hydration of CaO powder by gas–solid reaction

E. Serris [a,*], L. Favergeon [a], M. Pijolat [a], M. Soustelle [a], P. Nortier [b], R.S. Gärtner [c], T. Chopin [c], Z. Habib [c]

[a] Ecole Nationale Supérieure des Mines de Saint-Etienne, centre SPIN, LPMG FRE 3312 CNRS, 158 cours Fauriel 42023 Saint-Etienne, France
[b] LGP2, Grenoble INP, 461 rue de la Papeterie, 38402 Saint Martin d'Hères, France
[c] Lhoist Recherche et Développement SA, 31 rue de l'industrie, B-1400 Nivelles, Belgium

ARTICLE INFO

Article history:
Received 22 October 2010
Accepted 27 June 2011

Keywords:
Kinetics (A)
Hydration (A)
Microstructure (B)
CaO (D)
Anti-Arrhenius

ABSTRACT

Hydration of CaO powders by reaction with water vapor has been studied in isothermal and isobaric conditions. Experimental tests were performed within the temperature range of 70 °C–420 °C and with a water vapor pressure from 5 to 160 hPa by means of a thermogravimetric device. Two powders, exhibiting slight differences in their physical properties, were studied. However, for one of the powders and under some temperature and pressure conditions, the reaction is not complete. The difference of behavior between both CaO powders was interpreted by considering the effect of the morphological properties on the mechanism of growth of $Ca(OH)_2$.

1. Introduction

Hydration of calcium oxide (lime) by liquid water is a very well known reaction due to large domain of applications of hydrated calcium oxide in industry [1,2]. It is however surprising to see that only few papers have been published on the "dry" hydration of CaO or the interaction of water vapor with this oxide [3–6] in comparison with the recent growing interest of studies about CO_2 interactions on calcium oxides [7–9].

D.R. Glasson [3] studied the interaction of water vapor with different kinds of lime with specific surface areas from 1 to 100 $m^2.g^{-1}$ and he observed the agglomeration of particles during hydration at room temperature. A theoretical model for this reaction has been developed [4] with some experiments on CaO pellets at different water vapor pressure and temperature. They found that the two most important variables were the water vapor pressure and the calcination temperature. In some recent works [5,6] on CaO based sorbents, an anti-Arrhenius behavior was observed and the author linked this phenomenon to the initial content of CaO. They also studied the CaO hydration and $Ca(OH)_2$ decomposition over a multitude of cycles with as starting material crushed and sieved limestone ($CaCO_3$). The hydration rate decreased with increasing number of cycles.

The aim of this work is to reach a better knowledge of the mechanism of this reaction, studying the influence of the water pressure and temperature. Two distinct CaO powders were used under the same experimental conditions and the differences, observed on the curves giving the fractional extent of the reaction versus time, are discussed on the bases of the growth mechanism of the hydroxide and morphology of the two powders.

2. Materials and methods

2.1. Materials

The two types of powders used in this work were provided by Lhoist R&D SA. The first one was called "SBL" (Soft Burnt Lime) and the second one "HBL" (Hard Burnt Lime). The chemical analysis shows that SBL powder is composed of 94.7% in weight of CaO and HBL powder of 96.4% of CaO. The unburnt part is 2.8% in SBL instead of 0.7% in HBL. The other impurities are in the same proportions in both powders. Then the X-ray patterns show the standard peaks for well crystallized CaO (Halite structure) for both the SBL and the HBL sample (Fig. 1).

Particle size distributions (PSD) were obtained by means of laser diffraction performed on a Malvern Mastersizer 2000 and the results are shown in Fig. 2. Both distributions are mainly bimodal. Both products exhibit aggregates of about 70 μm and also small particles of less than 10 μm. The 90% cumulated mass fraction is 94 μm for SBL and 95 μm for HBL.

The specific surface area obtained by measuring nitrogen adsorption isotherms at 77K (BET method) with a micromeritics ASAP 2000 was found to be 1.42 ± 0.01 $m^2.g^{-1}$ for HBL sample and 2.16 ± 0.01 $m^2.g^{-1}$ for SBL sample. Comparing the equivalent diameter of the individual particles obtained from these values to the PSD results indicates that the bigger size peaks of Fig. 2 correspond to porous

* Corresponding author. Tel.: +33(0)477420290.
E-mail address: serris@emse.fr (E. Serris).

0008-8846/$ – see front matter © 2011 Elsevier Ltd. All rights reserved.
doi:10.1016/j.cemconres.2011.06.014

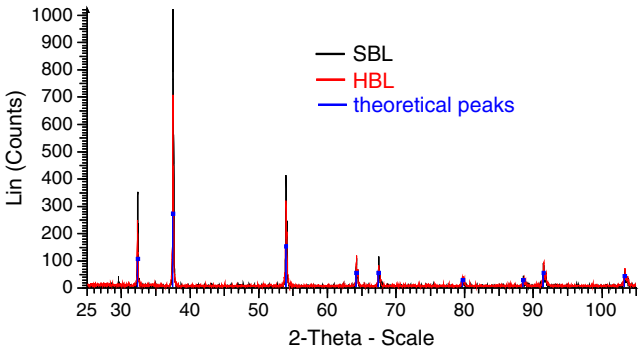

Fig. 1. XRD patterns of both powders.

aggregates of smaller particles. This has been confirmed by scanning electron microscopy (Jeol JSM 6500F) as shown in Fig. 3.

For SBL the number of small particle seems to be greater than for HBL, as shown by the PSD curves. Indeed, it is clear from Fig. 3 that the internal pores inside the SBL aggregates are larger than inside HBL ones.

This has been confirmed by pore volume distributions obtained by mercury intrusion porosimeter (Micromeritics Autopore IV). Fig. 4 shows the cumulative pore volume as a function of a pore diameter. We can notice both intra-granular and inter-granular voids. If we consider pores with diameters lower than 1 μm, it is clear that the pore volume inside the SBL aggregates (0.128 $mL.g^{-1}$) is much higher than that inside the HBL aggregates (0.042 $mL.g^{-1}$).

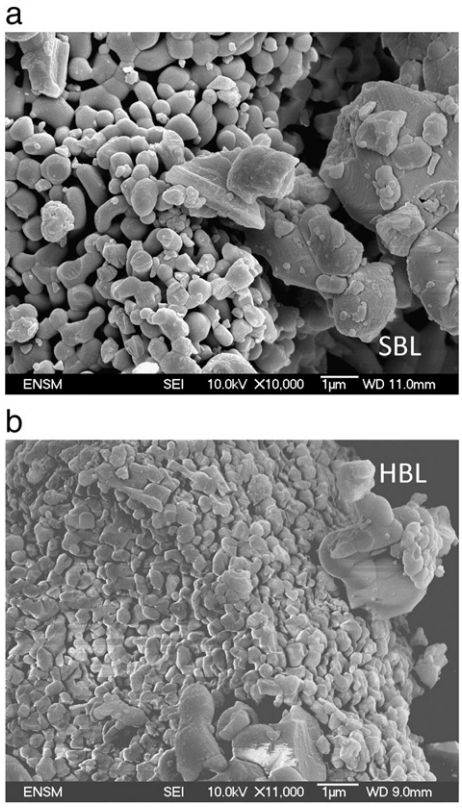

Fig. 3. Microstructure of the SBL (a) and the HBL (b) CaO aggregates.

2.2. Methods

All experiments have been performed at fixed temperature (T) and water vapor partial pressure (P) in a symmetrical thermobalance SETARAM TAG 24 associated with a water vapor generator Wetsys.

The procedure was the same for all thermogravimetric (TG) experiments. All experiments were realized in isobaric and isothermal conditions. The sample temperature was raised up to the isothermal step and then the gasses (helium and water vapor) were introduced. According to NIST data [10] the equilibrium pressure of calcium oxide hydration is represented in Fig. 5 by the plain curve.

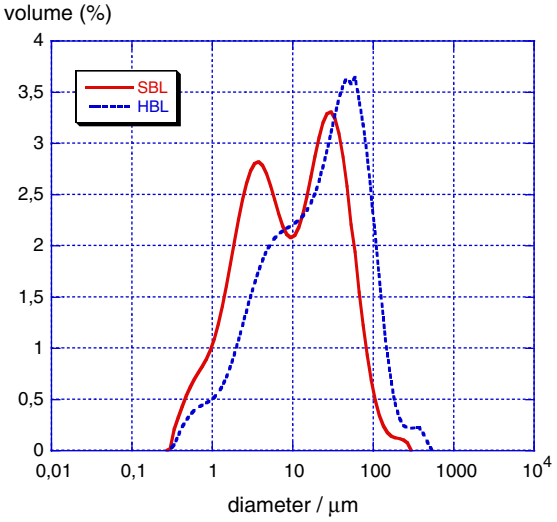

Fig. 2. Particle size distribution of the powders.

With the Wetsys vapor generator, we could achieve water vapor pressures up to 160 hPa in helium flux. So our experimental field is included in the hatched area between the equilibrium curve and the dotted lines. All the experiments have been carried out far from equilibrium conditions — so much so that the corresponding term in the expression of the rate can be left out. The TG software gave us mass variation versus time. We transformed this data into fractional extent α of the reaction according to the chemical reaction [R1]:

$$CaO(s) + H_2O(g) = Ca(OH)_2(s). \quad (R1)$$

The theoretical mass gain at $\alpha = 1$ should be of +32% of the initial mass of CaO. This initial mass is obtained after the experiment with a complete dehydration of $Ca(OH)_2$. Thus, we can calculate the hydrated part of the initial product.

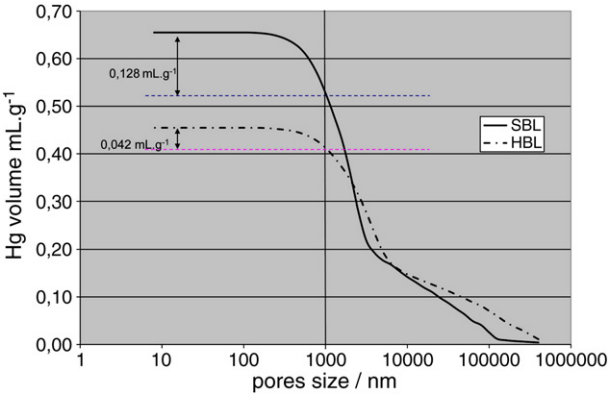

Fig. 4. Pore volume distribution as a function of pore diameter for SBL and HBL CaO powders.

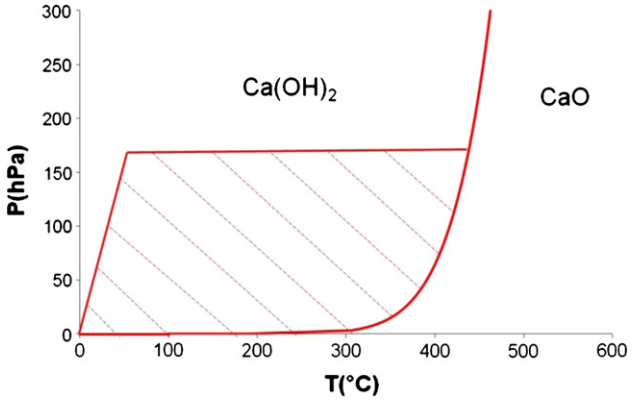

Fig. 5. Equilibrium pressure of hydration of calcium oxide and experimental exploration field.

Derivation of the α(t) curves allows us to calculate the rate of reaction (dα/dt), which can be represented graphically versus α, to compare the results of experiments carried out in various temperature and water pressure conditions.

3. Experimental results

3.1. Influence of water vapor pressure

The influence of the water vapor pressure on the kinetic curves is illustrated in Fig. 6. All experiments were realized with the SBL powder. The temperature was fixed at 150 °C for all tests.

According to the experimental α(t) curves, the higher the pressure, the faster the reaction (Fig. 6a). The maximal fractional extent observed for 80 and 160 hPa reaches mainly 1, which means that SBL powder can be totally transformed into $Ca(OH)_2$. The rate versus α curve exhibits a maximum for the higher pressure experiment. It seems that all the curves present such a maximum close to the initial time.

3.2. Influence of temperature

Fig. 7 shows α(t) curves obtained at various temperatures for SBL and HBL samples.

It can be seen that for both powders the higher the temperature, the slower the hydration. This can be observed from the dα/dt (α) curves shown in Fig. 8 for SBL CaO powder. Such a behavior is quite unusual.

We could also note that the maximum of the curves moves from α = 0.05 to nearly 0.4 when temperature increased.

3.3. Maximal extent of reaction: "blocking effect"

For HBL CaO powder and in some experimental conditions of dry hydration, the reaction was not complete and stopped at a fractional extent lower than 1. During the reaction something happen (for example a diffusion through the hydroxide layer became extremely slow) and the reaction rate is so slow that we can consider that the reaction is blocked. We will call this phenomenon the "blocking effect" in the following. Two curves of the fractional extent versus time are represented in Fig. 9 for two different temperatures with 5 hPa of water pressure.

The maximal value reached by the fractional extend depends for each powder on the operating conditions (temperature and water vapor pressure). Only HBL CaO powder exhibited such a behavior, as

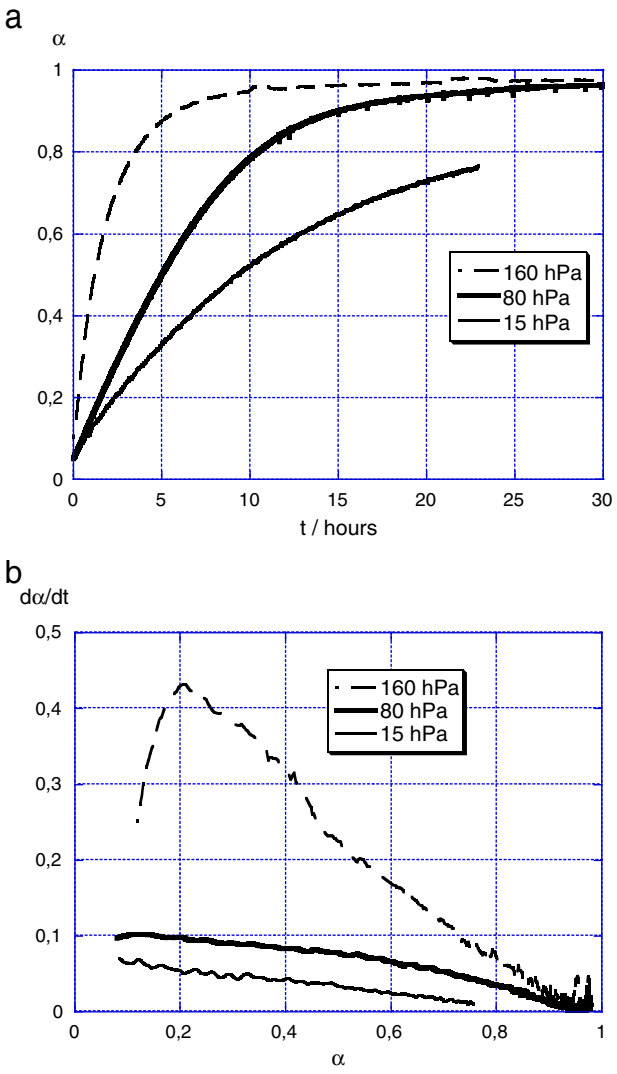

Fig. 6. Influence of water vapor pressure on the hydration of SBL CaO powders at 150 °C: α(t) (a) and dα/dt (b).

illustrated in Fig. 10. Same experimental conditions were use (115 °C, 5 hPa and 150 °C, 15 hPa) for both HBL and SBL experiments.

For HBL the blocking effect is clearly observed at 115 °C and 5 hPa since a plateau is reached for α equal to 0.7. In the other experiment (150 °C and 15 hPa), it can be foreseen that the fractional extent will not exceed 0.5. For SBL however, both reactions were not finished but the fractional conversion has reached values above 0.75 and does not seem to stop increasing well below 1.

4. Discussion, mechanism of the reaction

4.1. Kinetic laws

If we consider the hydration of SBL samples, the rate curves such as those in Fig. 6b or Fig. 8, exhibit a maximum, which suggests that the reaction involves simultaneous nucleation and growth processes of the new phase ($Ca(OH)_2$ in our case). In general [11], kinetic modeling of these reactions are done using a general expression of the reaction rate in the form $d\alpha/dt = A\exp(-\Gamma/RT).f(\alpha)$ where A is a pre-exponential factor, Γ a temperature coefficient called apparent activation energy in the literature, R the perfect gas constant, T the temperature and f(α) a function of the fractional conversion α (in the

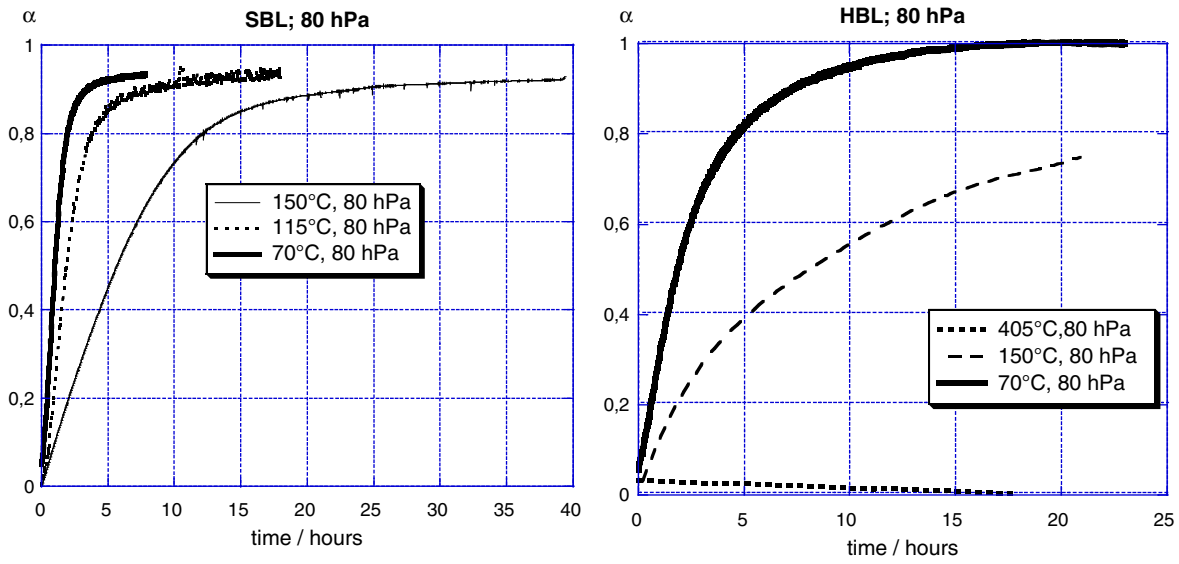

Fig. 7. Influence of temperature on hydration of SBL and HBL CaO powders with a water vapor pressure equal to 80 hPa.

case of sigmoid α(t) curves, authors often use the Avrami laws A_n or the Prout–Tompkins law B1). Nevertheless, Avrami laws and Prout–Tompkins law are not usable in the case of solid–gas reactions; and moreover the use of temperature dependence following an Arrhenius behavior should be done with care as explained in [12]. We use a more general method based on surface nucleation followed by nuclei growth [13]. This means that nuclei of hydroxide are formed onto the surface of the initial oxide grains with a frequency γ, called the areic frequency of nucleation and expressed in number of nuclei.$m^{-2}.s^{-1}$. The nuclei thus formed then grow with a rate ϕ called the areic reactivity of growth and expressed in mol.$m^{-2}.s^{-1}$. The most common laws used for such a behavior are those of either Mampel's [14,15] (uniform surface nucleation, isotropic growth, inward development and internal rate-determining step of growth) or of the different mechanisms with uniform nucleation and anisotropic growth as Jacobs and Tompkins' model for example [16,17]. Such models are explained and detailed in reference [18].

In this text, we will only consider a general form, $d\alpha/dt = \phi(P,T,\ldots).f(t)$ [19] if it is supposed that the growth rate is controlled by an elementary step. ϕ (T, P,...) will be expressed by the theoretical expression deduced from the mechanism of growth and this expression will help us to interpret experimental behavior (influence of temperature and partial pressure).

4.2. Proposal of a mechanism for growth and anti-Arrhenius behavior

For the growth of the calcium hydroxide layer, we refer to a traditional mechanism of solid–gas reaction taking into account both internal (between calcium hydroxide and calcium oxide) and external (between calcium hydroxide and water vapor) interfaces with diffusion of species through the hydroxide layer, with the specificity of the calcium hydroxide, which is insulating, and of water molecules which form easily hydrogen bonds while being likely to dissociate).

The various steps involved in the mechanism are detailed below:

At the external interface:

- The adsorption of water molecules with hydrogen bonds on two sites of adsorption (noted 's'):

$$H_2O + 2s \Leftrightarrow s{-}H_2O{-}s. \quad (S.1)$$

- The formation of an hydroxide group from an hydroxide vacancy:

$$s{-}H_2O{-}s + V_{OH}^{\bullet} \Leftrightarrow s{-}H^{\bullet} + OH_{OH} + s. \quad (S.2)$$

- The reaction between hydrogen and an oxygen ion in hydroxide position:

$$s{-}H^{\bullet} + O_{OH}^{'} \Leftrightarrow s + OH_{OH} \quad (S.3)$$

In the hydroxide layer:

- The diffusion of the hydroxide vacancy and of the oxygen ion from the internal interface toward the external interface

At the internal interface:

- The creation of the hydroxide vacancy and the oxygen ion in hydroxide position:

$$CaO \Leftrightarrow Ca_{Ca} + V_{OH}^{\bullet} + O_{OH}^{'}. \quad (S.4)$$

A linear combination of steps [S.1], [S.2], [S.3] and [S.4] leads to the overall reaction:

$$CaO(s) + H_2O(g) = Ca(OH)_2(s). \quad (R1)$$

The mechanism is solved by using the rate determining step method assuming that step [S.2] is the rate determining one [20]. We obtain for the areic reactivity of growth:

$$\phi = \phi_{[2]} = k_2[s{-}H_2O{-}s]\cdot[V_{OH}^{\circ}] \quad (E1)$$

We write that all the steps i, apart from [S.2], are at equilibrium with the corresponding equilibrium constant K_i and the electric neutrality:

$$\left[s{-}H^{\circ}\right] + \left[V_{OH^{\circ}}\right] = \left[O_{OH}^{'}\right]. \quad (E2)$$

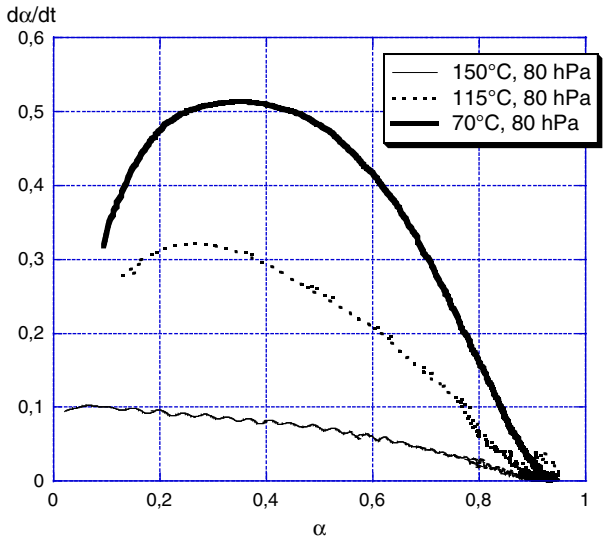

Fig. 8. Influence of the temperature on the kinetic rate of hydration of SBL CaO powder with a water vapor pressure of 80 hPa.

Assuming a low coverage of adsorption sites, that is: $[s-H_2O-s]<<1$ and $[s-H^+]<<1$, the areic reactivity of growth becomes:

$$\phi = k_2 K_1 K_4 P_{H_2O} \sqrt{\frac{K_3}{1 + K_3 K_4}}. \quad \text{(E3)}$$

According to this solution the areic reactivity of growth should not obey the Arrhenius law with temperature, which means that the temperature coefficient Γ does not have the meaning of an activation energy unless the condition $K_3K_4<<1$ is fulfilled. In this last case, the solution becomes:

$$\phi = k_2 K_1 K_4 \sqrt{K_3} P_{H_2O}. \quad \text{(E4)}$$

In this case, we can consider the temperature coefficient as an apparent activation energy connected to the activation energy E_2 of the rate determining step (formation of a hydroxide group from a hydroxide vacancy) and with the enthalpy ΔH_i of the various steps i constantly at equilibrium:

$$\Gamma = E_a = E_2 + \Delta H_1 + \frac{\Delta H_3}{2} + \Delta H_4. \quad \text{(E5)}$$

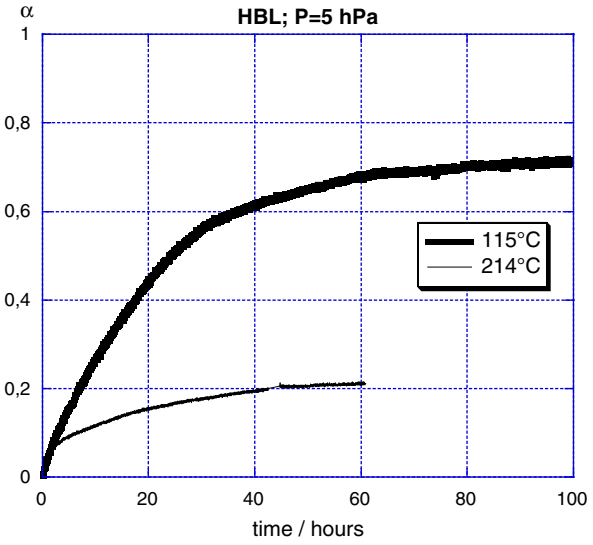

Fig. 9. Blocking effect for HBL powder.

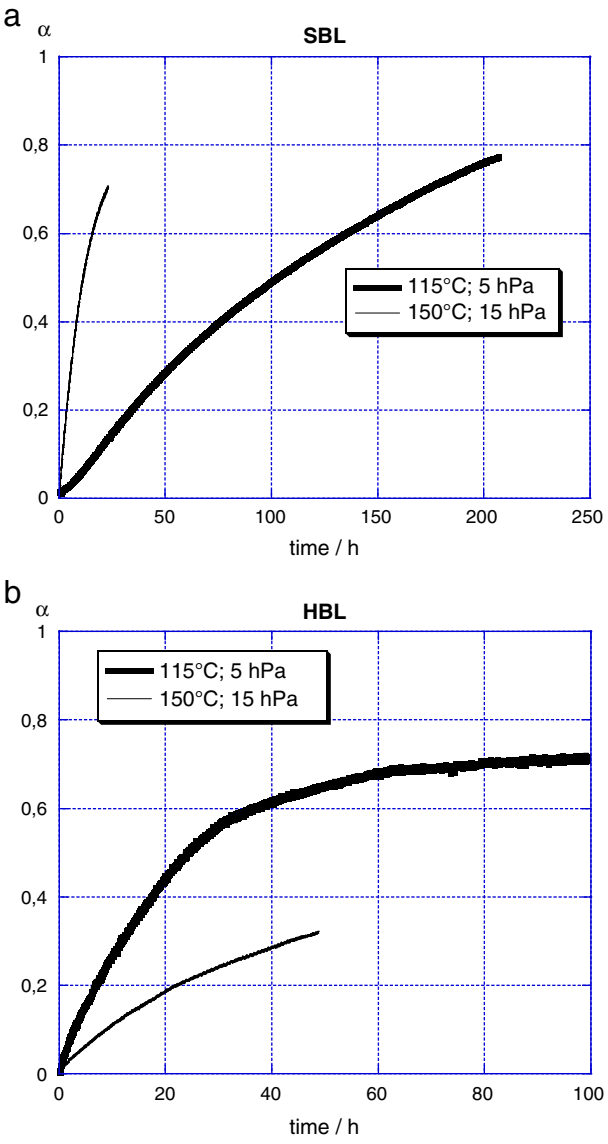

Fig. 10. Fractional conversion versus time incross over experiments on (a) SBL and (b) HBL CaO powders.

One can note, that there is indeed every chance that the preceding linear combination of the enthalpies is strongly negative, knowing that only the enthalpy of the rate determining step does not appear in the sum and that the total enthalpy of the reaction is strongly negative. Thus negative apparent activation energy is only the translation of strongly exothermic steps preceding the rate determining one. This property is known as an anti-Arrhenius behavior.

4.3. The blocking effect

In order to understand the origin of the blocking affect, the sample obtained at the end of the TG experiments were observed by SEM.

First, let's see the pictures of hydrated grains in an experiment with no blocking effect. Fig. 11 shows hydrated SBL after experiment at 160 °C and 160 hPa of water vapor pressure (no blocking effect).

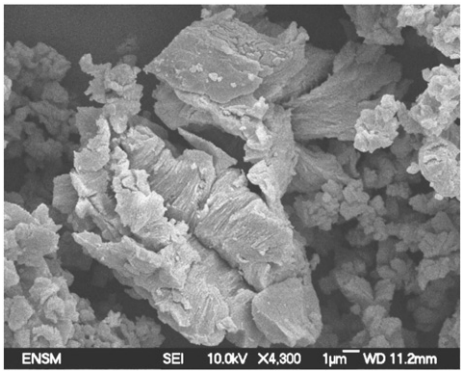

Fig. 11. SEM picture of hydrated SBL 115 °C, 5 hPa (no blocking effect).

All the grains in the initial aggregate were transformed into Ca $(OH)_2$ leading to an arrangement of grains with a gypsum flower like shape. A lamellar structure can be noticed with thin flakes of less than 50 nm. This microstructure is in agreement with the hexagonal crystalline structure of calcium dihydroxide. From observations of different hydrated SBL samples, aggregates in Fig. 11 as well as aggregates larger than 50 μm could be observed (cf Fig. 12). They are all composed of assemblies of the same gypsum flower pattern.

We can conclude from these observations that even if the transformation strongly modifies the microstructure of the initial particles, the global structure of the initial aggregates is not destroyed and they are still porous.

Fig. 13 shows the morphology of the aggregates (13b) and the surface of the aggregates (13a) in the case of a HBL sample hydrated at 115 °C and 5 hPa of water vapor pressure. For this sample, a blocking effect was observed with a value of 0.7 for the maximal fractional extent (cf Fig. 10b).

Aggregates look here very dense which is very different to the gypsum flower microstructure observed for the samples without blocking effect. It is not possible to distinguish individual grains like in the initial aggregates (cf Fig. 3b). Furthermore, some faces of the aggregates look very smooth suggesting that a continuous layer of Ca $(OH)_2$ had spread out without pore formation, only a few cracks were formed on these surfaces. On the other faces, however, the aggregates take more or less the lamellar microstructure previously observed with HBL, with some porosity.

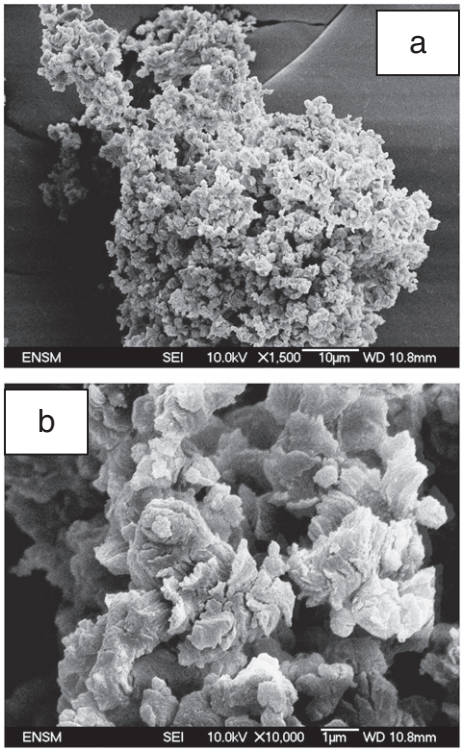

Fig. 12. SEM picture of hydrated SBL 160 °C, 80 hPa (no blocking effect): a) X 1500; b) X 10,000.

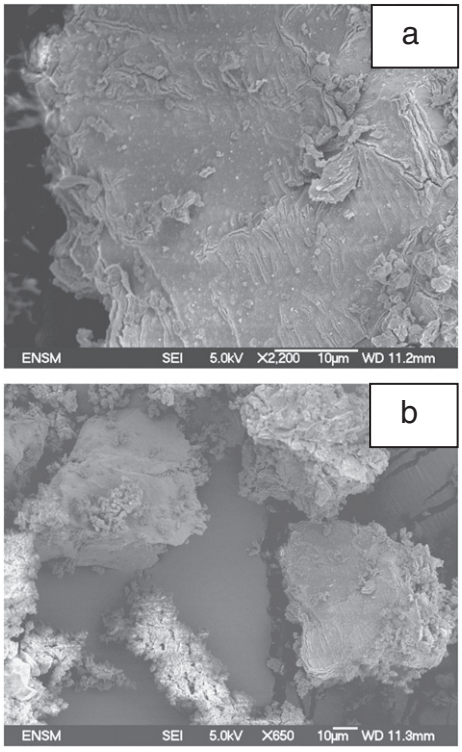

Fig. 13. SEM picture of hydrated HBL 115 °C, 5 hPa (blocking effect).

Considering the results obtained in the cross experiment (cf Fig. 10), the origin of the blocking effect may be attributed to the differences in the physical characteristics of both SBL and HBL CaO powders.

SEM observations reveal strong differences between SBL and HBL in the powder morphology after hydration: continuous superimposed layers for HBL with a global size slightly larger than the initial aggregates compared to individual grains transformed and gypsum flower pattern in the aggregates for SBL.

From these results we can imagine that the growth of $Ca(OH)_2$ may proceed according to two possible mechanisms. Indeed, calcium dihydroxide crystallizes in hexagonal structure (space group P3m1), which presents a strong anisotropy. So two directions of growth may be considered: either perpendicular or parallel to the hexagonal planes of the $Ca(OH)_2$ structure. Fig. 14 illustrates schematically the differences in both possible mechanisms.

The so-called perpendicular growth proceeds quite usual in gas–solid reactions: according to the mechanism described above and the inward advance of the internal interface. In the parallel mechanism, after the adsorption, the diffusion of calcium and oxygen ions may proceed from the internal interface by the side of the hexagonal planes of $Ca(OH)_2$, thus leading to their possible extension by reacting with hydroxyls and proton ions present at the surface. This second way of Ca $(OH)_2$ growth better explains the gypsum flower microstructure observed by SEM in the hydrated samples. Thus the parallel mechanism seems to be predominant in both kinds of powders. However, the perpendicular one may occur too, at least in the firsts moments of the reaction, and as long as the thickness of $Ca(OH)_2$ layer remains low. In such anisotropic crystals, the diffusion in the direction perpendicular to the layers is generally slow compared to surface diffusion, especially at

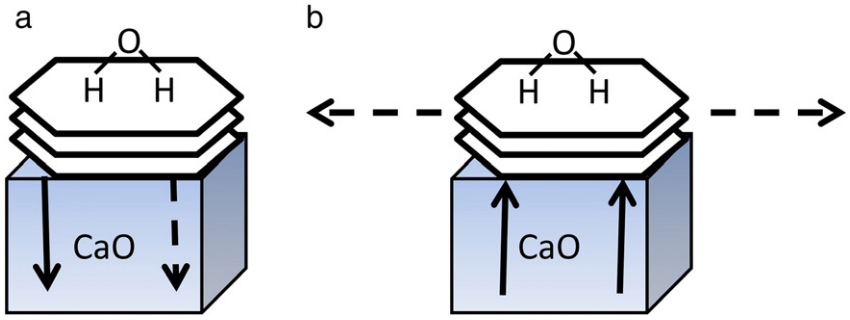

Fig. 14. Schemes of perpendicular (a) and parallel (b) growth processes. Bold and dashed arrows indicate the direction of diffusing species and of development of $Ca(OH)_2$, respectively.

the temperatures investigated in this study (lower than 420 °C). In the case of SBL powder, where numerous open pores exist inside the aggregates, the reaction takes place in each particle separately, without interaction with the neighboring particles. Thus the water vapor may easily circulate inside the porosity, which is in favor of a total conversion of CaO into $Ca(OH)_2$. On the other hand, since the HBL powder is composed of very compact aggregates, the parallel growth leads to much more continuous layers of $Ca(OH)_2$, which tend to envelop very large areas of the aggregates. As a consequence, the access of the reacting gas inside the aggregates is strongly reduced, and it results in an incomplete transformation, the perpendicular growth being too sluggish in the temperature range investigated (up to 420 °C).

5. Conclusions

CaO hydration by water vapor has been investigated using thermogravimetry at constant temperature and water partial pressure. The curves of the fractional extent versus time obtained for two distinct CaO powders revealed several interesting features:

- the influence of water vapor pressure enhanced the kinetics of reaction with a linear dependence of the pressure on the rate;
- an anti-Arrhenius behavior was observed for the temperature dependence, due to extremely exothermic reaction combined with a rate determining step leading to an expression of the rate including all the steps;
- a "blocking effect" was also observed for only one of the powders (less inter aggregate porosity) with "in fine" packed aggregates attributed to the growth of $Ca(OH)_2$ continuous layers around the aggregates.

References

[1] H. Shi, Y. Zhao, W. Li, Cem. Concr. Res. 32 (5) (2002) 789–793.
[2] J.-M. Commandré, S. Salvadora, A. Nzihoua, Chem. Eng. Res. Des. 85 (4) (2007) 473–480.
[3] D.R. Glasson, J.appl.Chem. 8 (1958) 798–803.
[4] A. Maciel Camacho, H.R. Hernandez, A.W.D. Hills, et al., Isij Int. 37 (5) (1997) 468–476.
[5] S. Lin, Y. Wang, Y. Suzuki, Energy Fuels 23 (2009) 2855–2861.
[6] Y. Wang, S. Lin, Y. Suzuki, Effect of CaO, Fuel Process. Technol. 89 (2008) 220–226.
[7] P. De Silva, L. Bucea, D.R. Moorehead, V. Sirvivatnanon, Cem. Concr. Comp. 28 (2006) 613–620.
[8] K.B. Yi, C.H. Ko, J.H. Park, et al., Catalysis Today 146 (1–2) (2009) 241–247.
[9] V. Manovic, J.P. Charland, J. Blamey, et al., Fuel 88 (10) (2009) 1893–1900.
[10] ChaseM.W. Jr., NIST-JANAF themochemical tables, fourth edition, J. Phys. Chem. Ref. Data, Monograph 9 (1998) 1–1951.
[11] A.K. Galwey, M.E. Brown, Thermal Decomposition of Ionic Solids, Elsevier, 1999.
[12] M. Pijolat, L. Favergeon, M. Soustelle, Thermochimica acta (2011) (submitted).
[13] M. Soustelle, Handbook of heterogeneous kinetics, ISTE - Wiley, London, 2010 edited by.
[14] K.L. Mampel, Z. Phys. Chem., Abt. A 187 (1940) 235–249.
[15] W.A. Johnson, R.F. Mehl, Trans. Amer. Inst. Mining Met. Eng. 135 (1939) 416–442.
[16] P.W.M. Jacobs, F.C. Tompkins, Chemistry of the Solid State, in: W.E. Gardner (Ed.), Butterworths Scientific Publications, London, 1955, p. 203.
[17] P.W.M. Jacobs, J. Phys. Chem. B 101 (1997) 10086–10093.
[18] M. Soustelle, Handbook of heterogeneous kinetics, edited by ISTE - Wiley, London, 2010, pp. 351–370.
[19] M. Pijolat, M. Soustelle, Experimental tests to validate the rate-limiting step assumption used in the kinetic analysis of solid-state reactions, Thermochimica acta 478 (2008) 34–40.
[20] M. Soustelle, Handbook of heterogeneous kinetics, edited by ISTE - Wiley, London, 2010, pp. 220–233.